Research Article

Improved NIR emission from Tb^{3+}, Yb^{3+} and Nd^{3+} co-doped La_2O_3 nano-phosphor

Neha Jain[1] · Rajan Kumar Singh[1] · Khalid Bin Masood[1] · Jai Singh[1,2]

Received: 10 December 2019 / Accepted: 4 February 2020 / Published online: 14 February 2020

Abstract
NIR and visible emission have been reported from Tb^{3+}, Nd^{3+} and Yb^{3+} doped La_2O_3. XRD, TEM and HRTEM corroborate good crystallinity of the nano-phosphor. The average particle size is around 15 nm examined via TEM and HRTEM. The photoluminescence up-conversion spectra of Tb^{3+} and Yb^{3+} co-doped La_2O_3 exhibited characteristic emission peaks of Tb^{3+} ion at 480, 544 and 610 nm. It is possible due to the absorption of two 980 nm pump photons by Tb^{3+} ion via Yb^{3+} sensitizer. The energy migration from Tb^{3+} to Nd^{3+} takes place so that the intensity of 820 nm ($^4F_{5/2}$, $^2H_{9/2} \rightarrow {}^4I_{9/2}$) is increased significantly. The energy transfer between these two ions reduces the intensity of 544 nm Tb^{3+} ion whereas the intensity of 820 nm improved. Energy transfer mechanism between Tb^{3+}, Nd^{3+} and Yb^{3+} ions has been discussed in detail. It would be a promising candidate for solar cells and biomedical applications.

Keywords La_2O_3 · X-ray diffraction · Energy transfer · Phosphors

1 Introduction

The maximum loss in solar cells occurs due to the passage of lower energy photon through it without creating an electron–hole pair (exciton) and also due to the high energy photons which cause thermal loss at the junction [1]. Lanthanide activated phosphors garnered much attention because these convert energy from higher to lower unit and vice versa [2–5]. Solar cells are divided into various categories namely c-Si, amorphous solar cells, dye-sensitized and organic–inorganic solar cells and their band gap is found in the range 1.1–1.8 eV (~650 to 1100 nm). It is previously reported that Nd^{3+}, Tb^{3+}, Ce^{3+}, Eu^{3+}, Tm^{3+} co-doped with Yb^{3+} ion gives emission around ~800 to 1000 nm via ultra-violet or visible excitation [3–7]. However, recent researches are focused on the development of such type of phosphor materials which significantly absorb infrared and UV–visible radiation. These absorbed radiations are converted into the radiations comparable to the solar cell band gap. Nd^{3+} ion would absorb UV–visible as well as NIR photons and it could be sensitized through Yb^{3+} ion [4, 8]. Additionally, Yb^{3+} co-doped Tb^{3+} also gives up-conversion (UC) green emission [9]. Prorok et al. [10] reported energy migration up-conversion from Tb^{3+} to Yb^{3+} and Nd^{3+} co-doped fluoride core–shell structure. La_2O_3 is a promising host for rare-earth doping because it has low phonon energy which significantly reduces the possibility of non-radiative (NR) transitions [11]. Also, it is compatible with other fluorescent lanthanides which also reduce the possibility of non-radiative transitions. Chen et al. [12] reported $LiYF_4$: Yb^{3+}, Er^{3+} single crystal to improve the power conversion efficiency of perovskite solar cell. Here, we report photoluminescence (PL) UC-emission by Tb^{3+}, Yb^{3+} and Nd^{3+} co-doped La_2O_3. The samples were synthesized by the polyol method. The NIR emission intensity of 820 nm (Nd^{3+} ion) might be improved due to energy migration from Tb^{3+} and Yb^{3+} ions.

✉ Jai Singh, jai.bhu@gmail.com | [1]Department of Physics, Dr. Harisingh Gour University, Sagar, MP 470003, India. [2]Department of Physics, Guru Ghasidas University, Bilaspur, CG, India.

2 Experimental method

La_2O_3 (99.9%), Tb_2O_3 (99.98%), Yb_2O_3 (99.995%) were purchased from Alfa Aesar. Nd_2O_3 (99.9%), ethylene glycol, urea and HNO_3 (69%) were purchased from Merck. $La(NO_3)_3$, $Tb(NO_3)_3$, $Nd(NO_3)_3$ and $Yb(NO_3)_3$ were prepared by dissolving their respective oxides in de-ionized water with the addition of few drops of HNO_3. The nitrate was mixed by taking the solution of $La(NO_3)_3$, $Tb(NO_3)_3$ $Yb(NO_3)_3$ and $Nd(NO_3)_3$ in a volumetric flask. Another solution was prepared by dissolving 4 g urea in 25 ml ethylene glycol (pH around 8–9). This solution is added to the rare earth nitrate solution kept at continuous stirring at the temperature of 120 °C for 4 h to complete the precipitation. The precipitate obtained was washed with de-ionized water and methanol and then dried it at 80 °C. Finally, the sample was calcined at 800 °C for the phase formation of La_2O_3. The structural analysis was characterized by using D8 Bruker X-ray diffractometer (XRD) with Ni-filtered Cu-Kα (1.5405 Å) radiation ($10° < 2\theta < 80°$ with a step size of 0.02°). The morphology of particles was determined by using the transmission electron microscope (TECNAI G2, 300 keV). The up-conversion spectra were recorded by exciting with diode laser 980 nm (CW, 1 W) using an iHR320 Jobin–Yvon spectrometer equipped with R928 photomultiplier tube. The PL decay measurement for a 544 nm emission band was performed with a 980 nm diode source. The collected signal was interfaced to a 150 MHz digital oscilloscope (model no. HM 1507, Hameg Instruments).

3 Results and discussion

Figure 1a shows XRD pattern of La_2O_3: 1%Tb, 10%Yb, x % Nd (x = 5, 10 at%) nanoparticles. All the diffraction peaks match with JCPDS 65-3185 reflecting the cubic phase (space group $Ia\bar{3}$) of La_2O_3 (a = 11.42 Å and V = 1489.36 $Å^3$). Absence of impurity phases corroborates successful substitution of La^{3+} with Tb^{3+}, Nd^{3+} and Yb^{3+} ions. However, a diffraction peak splits into two parts in which a peak mark by * at 27.96° obtained due to the formation of La_2O_3 cubic structure and space group $Im\bar{3}m$ from JCPDS card number

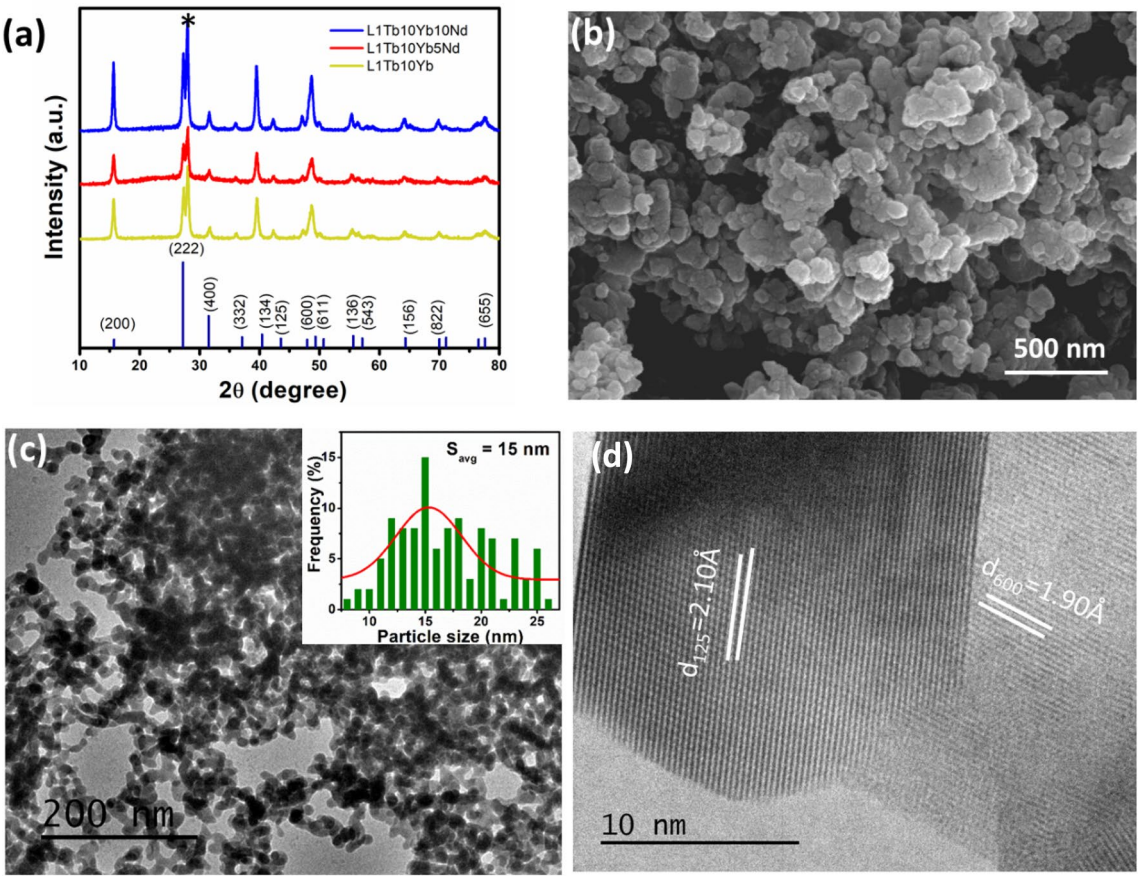

Fig. 1 **a** XRD pattern of La_2O_3: 1%Tb^{3+}, 10% Yb^{3+}, x % Nd^{3+} (x = 0, 5, 10) with JCPDS data 65-3185, **b** SEM image, **c** TEM image (inset particle distribution plot) and **d** HRTEM of La_2O_3: 1%Tb^{3+}, 10%Yb^{3+}

89-4016. The broadness of the peaks shows the formation of nano-particle with good crystallinity. The crystalline size was lies in the range 6–8 nm which was calculated by Scherrer formula. Moreover, the morphology and size of the particles is determined by SEM and TEM which is shown in Fig. 1b, c. The particles are spherical in shape, uniformly distributed and exhibit particle size of around 8–26 nm. In addition, the particle size distribution plot is shown in the inset of Fig. 1c. The average particle size estimated from Gaussian fitting is 15 nm. The corresponding high-resolution TEM (HRTEM) is given in Fig. 1d. It is indexed according to JCPDS file representing (125) and (600) planes of La_2O_3. There are no defects or absence of grain boundaries found in HRTEM.

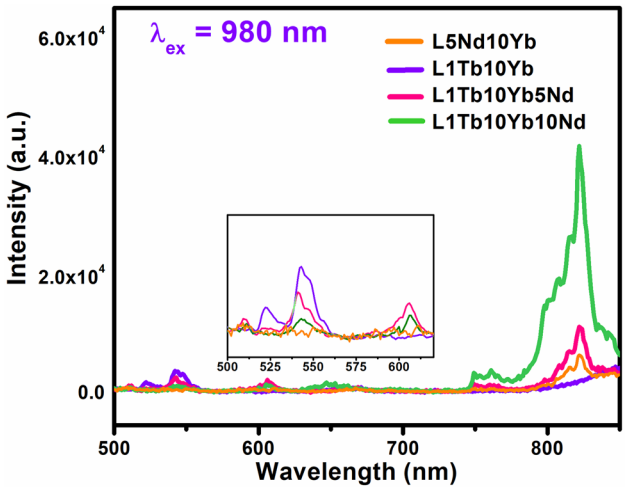

Fig. 2 Up-conversion PL emission spectra of 1%Tb^{3+} and 10%Yb^{3+}, x%Nd^{3+} (x = 0, 5, 10%) co-doped La_2O_3 (λ_{ex} = 980 nm). Inset show PL spectra in visible region

PL emission spectra recorded under 980 nm excitation of Tb^{3+} and Yb^{3+} co-doped La_2O_3 shows emission peaks of Tb^{3+} at 544 ($^5D_4 \rightarrow {}^7F_5$), 610 nm ($^5D_4 \rightarrow {}^7F_3$) shown in Fig. 2 [2]. The dominant intensity was observed for 544 nm emission. Nd^{3+} co-doped La_2O_3 exhibits Tb^{3+} as well as Nd^{3+} emission peaks. The emission peaks are centered at 760 and 820 nm observed due to $^4S_{3/2} \rightarrow {}^4I_{9/2}$ and $^4F_{5/2}$, $^2H_{9/2} \rightarrow {}^4I_{9/2}$ transitions, respectively [8, 13, 14]. From PL emission spectra it is clearly shown that the intensity of 820 nm emission increases with increasing Nd^{3+} concentration. However, from the inset of Fig. 2, it can be interpreted that the intensity of 544 nm emission decreases with increasing Nd^{3+} concentration. It might be due to the energy migration from Tb^{3+} ion to Nd^{3+} ion so that the intensity of 820 nm would improve. Yb^{3+} also transfers its energy to Nd^{3+} so that UC emission is possible from the sample. However, the intensity of other peaks of Tb^{3+} ion is not much affected by Nd^{3+} doping. Tb^{3+} ion also gives emission with UV-excitation and it transfers its absorbed energy to Nd^{3+} ion. So present phosphor also able to reduce heating loss from solar cell junction because could absorb UV-radiation and convert into NIR radiation (820 nm) comparable to the solar cell band gap. Moreover, if the number of photons absorbed by solar cells increases than the efficiency of solar cells obviously increases.

The number of photons involved in the emission process is calculated by using the relation $I \alpha P^n$ where I is the integrated area, P is pumped laser power and n is the number of significant photons involved for single-photon emission [15]. Figure 3a, b represents power-dependent emission spectra and ln(I) versus ln (P) plot for of La_2O_3: 1% Tb^{3+}, 10% Yb^{3+}, 5% Nd^{3+}. The slope of the logarithmic graph indicates the number of significant photons involved for 543 and 820 nm emission. It is 1.03 for Nd^{3+} ions 820 nm emission and 1.47 for Tb^{3+} ions 544 nm

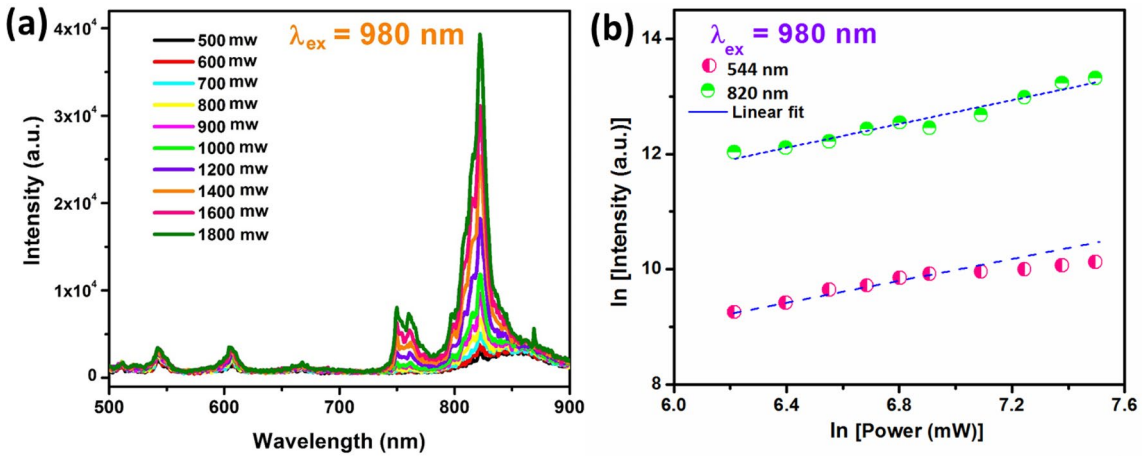

Fig. 3 **a** Power dependent emission spectra of La_2O_3:1%Tb^{3+}, 10%Yb^3, 5%Nd^{3+} and **b** its logarithmic dependent pump power versus integrated intensity of 544 nm and 820 nm emission

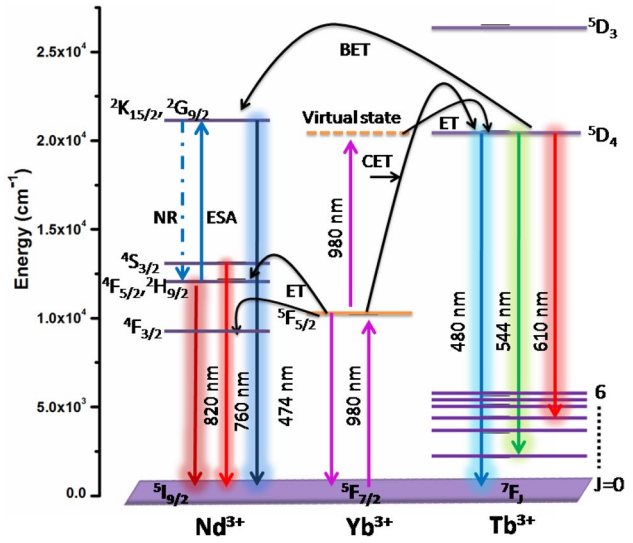

Fig. 4 Schematic UC energy level diagram at 980 nm excitation

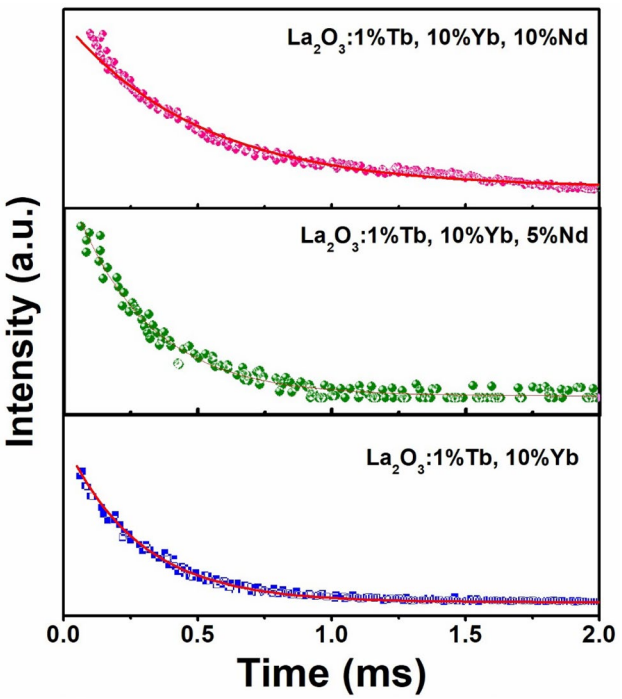

Fig. 5 Decay time measurement for La_2O_3: 1%Tb^{3+}, 10% Yb^{3+}, x% Nd^{3+} (x = 0, 5, 10) at λ_{em} = 544 nm and λ_{ex} = 980 nm

emission. Nearly two photons are absorbed by Tb^{3+} ion for green emission whereas only one photon is needed for 820 nm emission [16, 17]. Tb^{3+} ion gets excited via absorbing a 980 nm pump photon by excited-state absorption or energy transfer UC process through Yb^{3+} sensitizer. However, Nd^{3+} absorbs energy from Tb^{3+} ion ($^5D_4$ state) and gets excited to $^4S_{3/2}/^4F_{5/2}/^2H_{9/2}$ state then relaxes to ground state ($^4I_{9/2}$) by emitting visible and NIR photons.

Figure 4 illustrates schematic energy level diagram for energy transfer (ET) between Tb^{3+}, Nd^{3+} and Yb^{3+} ions. When 980 nm photon incidents on the sample, Yb^{3+} absorbs that photon and get excited to $^5F_{5/2}$ state. Yb^{3+} absorbs another 980 nm photon in its excited state ($^5F_{5/2}$) and get populate to its virtual excited state. The energy of Yb^{3+} ions virtual excited state is approximately equal to the energy of the $^5D_4$ state of Tb^{3+} ion. Therefore, Tb^{3+} ions electrons get excited to $^5D_4$ state by co-operative energy transfer (CET) then relaxe to the ground by emitting visible photons. Meanwhile, Tb^{3+} also transfers its energy to Nd^{3+} ion by back energy transfer (BET) which is supported from PL emission spectra given in inset of Fig. 2 [10, 18]. Moreover, some electrons excite from excited-state absorption (ESA) to $^2G_{9/2}$ state in Nd^{3+} and electrons transit from this state to $^4F_{5/2}$ NR relaxation. Simultaneously, energy transfer between $^5F_{5/2}$ (Yb^{3+}) and $^4F_{5/2}/^4F_{3/2}$ (Nd^{3+}) also takes place so that more electron gets populated in $^4F_{5/2}$ state of Nd^{3+} ion. Then it relaxes to the ground state by an emitting photon of 820 nm radiation.

The lifetime of the sample has been measured for 544 nm emission and 980 nm excitation wavelength. The decay profile is shown in Fig. 5 for Tb^{3+}–Yb^{3+} and Nd^{3+} co-doped sample. The decay time estimated by the mono-exponential fitting equation $I = I_0\, e^{-t/\tau 1}$, where I_0 is the initial intensity and τ is the lifetime. Here, lifetime values observed from mono-exponential fitting are 0.42, 0.34 and 0.23 ms for La_2O_3:1%Tb^{3+}, 10%Yb^{3+}, La_2O_3:1%Tb^{3+}, 10%Yb^3, 5%Nd^{3+} and La_2O_3:1%Tb^{3+}, 10%Yb^3, 10%Nd^{3+}. The energy transfer efficiency from Tb^{3+} ion to Nd^{3+} was calculated by using the following equation:

$$\eta = 1 - \frac{\tau}{\tau_0} \tag{1}$$

where η is energy transfer efficiency from Tb^{3+} ion to Nd^{3+} ion, τ is the lifetime in presence of acceptor Nd^{3+} ion, τ_0 an average lifetime of sensitizer (Tb^{3+} ion). From this equation maximum transfer efficiency observed for La_2O_3:1%Tb^{3+}, 10%Yb^3, 10%Nd^{3+} is 45.6% which represents that Tb^{3+} efficiently transfer energy to Nd^{3+} ion.

4 Conclusions

Tb^{3+}, Nd^{3+} and Yb^{3+} doped exhibiting cubic structure have been successfully synthesized. UC PL emission spectra indicate improvement in emission intensity of 820 nm of Nd^{3+} ion due to absorption of energy from both Yb^{3+} and Tb^{3+} ions. The enhancement is observed due to migration of energy between lanthanides. Moreover, reduction in intensity of 544 nm confirms energy transfer from Tb^{3+} to Nd^{3+} ion. These studied reveals that Yb^{3+} co-doping

improves up-conversion performance of nano-phosphors. Tb^{3+} also transfers its energy to Nd^{3+} ion so its emission would significantly improve which is beneficial for improving solar cell efficiency.

Acknowledgements Authors are thankful to Sophisticated Instrument centre of the University for providing various characterization facilities. We are also thankful to Prof. S.B. Rai for providing PL facility. Neha Jain acknowledges the Maulana Azad National Fellowship provided by University Grants Commission (UGC), Govt. of India. Jai Singh would like to acknowledge UGC-India and DST for providing project under UGC Start-up Grant FT30 [HYPHEN]56/2014 (BSR)3(A) a and DST Fast track Grant No. SR/FTP/PS[HYPHEN]144/2012.

Compliance with ethical standards

Conflict of interest On behalf of all authors, the corresponding author states that there is no conflict of interest.

References

1. Ramasamy P, Manivasakan P, Kim J (2014) Upconversion nanophosphors for solar cell applications. RSC Adv 4:34873–34895
2. Jain N, Singh BP, Singh RK, Singh J, Singh RA (2017) Enhanced photoluminescence behaviour of Eu^{3+} activated $ZnMoO_4$ nanophosphors via Tb^{3+} co-doping for light emitting diode. J Lumin 188:504–513
3. Singh BP, Singh J, Singh RA (2014) Luminescence properties of Eu^{3+}-activated $SrWO_4$ nanophosphors-concentration and annealing effect. RSC Adv 4:32605–32621
4. Song D, Guo C, Zhao J, Suo H, Zhao X, Zhou X, Liu G (2016) Host sensitized near-infrared emission in Nd^{3+}–Yb^{3+} Co-doped $Na_2GdMg_2V_3O_{12}$ phosphor. Ceram Int 42:12988–12994
5. Terra IAA, Borrero-González LJ, Figueredo TR, Almeida JMP, Hernandes AC, Nunes LAO, Malta OL (2012) Down-conversion process in Tb^{3+}–Yb^{3+} co-doped Calibo glasses. J Lumin 132:1678–1682
6. Li J, Chen L, Hao Z, Zhang X, Zhang L, Luo Y, Zhang J (2015) Efficient near-infrared downconversion and energy transfer mechanism of Ce^{3+}/Yb^{3+} codoped calcium scandate phosphor. Inorg Chem 54:4806–4810
7. Yu T, Lin H, Yu D, Ye S, Zhang Q (2015) Energy transfer dynamics and quantum Yield derivation of the Tm^{3+} concentration-dependent, three-photon near-infrared quantum cutting in La_2BaZnO_5. J Phys Chem C 119:26643–26651
8. Sun J, Sun Y, Cao C, Xia Z, Du H (2013) Near-infrared luminescence and quantum cutting mechanism in $CaWO_4$:Nd^{3+}, Yb^{3+}. Appl Phys B 111:367–371
9. Dong H, Sun L, Wang Y, Xiao J, Tu D, Chen X, Yan C (2016) Photon upconversion in Yb^{3+}–Tb^{3+} and Yb^{3+}–Eu^{3+} activated core/shell nanoparticles with dual-band excitation. J Mater Chem C 4:4186–4192
10. Prorok K, Pawlyta M, Strek W, Bednarkiewicz A (2016) Energy migration up-conversion of Tb^{3+} in Yb^{3+} and Nd^{3+} codoped active-core/active-shell colloidal nanoparticles. Chem Mater 28:2295–2300
11. Xu Z, Bian S, Wang J, Liu T, Wang L, Gao Y (2013) Preparation and luminescence of La_2O_3:Ln^{3+} (Ln^{3+} = Eu^{3+}, Tb^{3+}, Dy^{3+}, Sm^{3+}, Er^{3+}, Ho^{3+}, Tm^{3+}, Yb^{3+}/Er^{3+}, Yb^{3+}/Ho^{3+}) microspheres. RSC Adv 3:1410–1419
12. Chen X, Xu W, Song H, Chen C, Xia H, Zhu Y, Zhou D, Cui S, Dai Q, Zhang J (2016) Highly efficient $LiYF_4$:Yb^{3+}, Er^{3+} upconversion single crystal under solar cell spectrum excitation and photovoltaic application. ACS Appl Mater Interfaces 8:9071–9079
13. Marciniak L, Bednarkiewicz A, Drabik J, Trejgis K, Strk W (2017) Optimization of highly sensitive YAG: Cr^{3+}, Nd^{3+} nanocrystal-based luminescent thermometer operating in an optical window of biological tissues. PCCP 19:7343–7351
14. Marciniak L, Bednarkiewicz A, Stefanski M, Tomala R, Hreniak D, Strek W (2015) Near infrared absorbing near infrared emitting highly-sensitive luminescent nanothermometer based on Nd^{3+} to Yb^{3+} energy transfer. Phys Chem Chem Phys 17:24315–24321
15. Singh BP, Parchur AK, Singh RK, Ansari AA, Singh P, Rai SB (2013) Structural and up-conversion properties of Er^{3+} and Yb^{3+} co-doped $Y_2Ti_2O_7$ phosphors. Phys Chem Chem Phys 15:3480–3489
16. Pandey A, Rai VK, Kumar V, Kumar V, Swart HC (2015) Upconversion based temperature sensing ability of Er^{3+}–Yb^{3+} codoped $SrWO_4$: an optical heating phosphor. Sens Actuators B 209:352–358
17. Hu F, Wei X, Qin Y, Jiang S, Li X, Zhou S, Chen Y, Duan CK, Yin M (2016) Yb^{3+}/Tb^{3+} co-doped $GdPO_4$ transparent magnetic glass-ceramics for spectral conversion. J Alloys Compd 674:162–167
18. Deshmukh P, Satapathy S, Ahlawat A, Tiwari MK, Karnal AK (2018) Fabrication and characterization of Er, Nd codoped Y_2O_3 transparent ceramic: a dual mode photoluminescence emitter. J Alloys Compd 754:32–38